

Fault-Tolerant Masked Matrix Accumulation using Bulk Bitwise In-Memory Engines

João P. C. de Lima^{1,2}, Benjamin F. Morris III³, Asif Ali Khan¹, Jeronimo Castrillon^{1,2,4}, Alex K. Jones⁵

TU Dresden¹, ScaDS.AI², Duke University³, Barkhausen Institut⁴, Syracuse University⁵

Email(s): joao.lima@tu-dresden.de, akj@syr.edu

Abstract—Big data processing has exposed the limits of compute-centric hardware acceleration due to the memory-to-processor bandwidth bottleneck. Consequently, there has been a shift towards memory-centric architectures, leveraging substantial compute parallelism by processing using the memory elements directly. Computing-in-memory (CIM) proposals for both conventional and emerging memory technologies often target massively parallel operations. These range from analog dot-product computations with research-stage memristor crossbars to simple, large-scale bitwise operations using commodity DRAM. However, current CIM solutions face significant challenges. For emerging data-intensive applications, such as advanced machine learning techniques and bioinformatics, where matrix multiplication is a key primitive, memristor crossbars suffer from limited write endurance and expensive write operations. In contrast, while DRAM-based solutions have successfully demonstrated multiplication using additions, they remain prohibitively slow.

This paper introduces Count2Multiply, a technology-agnostic digital-CIM method for performing integer-binary and integer-integer matrix multiplications using high-radix, massively parallel counting implemented with bitwise logic operations. In addition, Count2Multiply is designed with fault tolerance in mind and leverages traditional scalable row-wise error correction codes, such as Hamming and BCH codes, to protect against the high error rates of existing CIM designs. We demonstrate Count2Multiply with a detailed application to CIM in conventional DRAM due to its ubiquity and high endurance. We also explore the acceleration potential of racetrack memories due to their shifting properties, which are natural for Count2Multiply, and their high endurance. Compared to the state-of-the-art in-DRAM method, Count2Multiply achieves up to $10\times$ speedup, $3.8\times$ higher GOPS/Watt, and $1.4\times$ higher GOPS/area, while the RTM counterpart offers gains of $10\times$, $57\times$, and $3.8\times$.

I. INTRODUCTION

Multiply and accumulate (MAC) is a fundamental computational primitive in many data-intensive high-performance computing, machine learning, bioinformatics, and cryptography applications. GPUs, TPUs, FPGAs, and other accelerators address these applications' needs with parallel execution units and/or integrated specialized MAC units. Despite delivering throughput in the PetaFLOPs (PFLOPs) range, these architectures are energy-hungry and remain bounded by memory bottleneck due to their compute-centric nature [7]. Consequently, there is a growing trend towards compute-in-memory (CIM) solutions [1]. CIM has gained particular attention because emerging workloads often require only low precision integer-integer (≤ 8 bits), integer-binary, or integer-ternary operations for sufficient accuracy [31], [34], [37].

In recent years, several works have leveraged DRAM [16], [52], SRAM [15], and emerging non-volatile memory technologies (NVMs) like STT-MRAM [19], PCM [60], RRAM [59], FeFET [26], and racetrack memory (RTM) [6] for in-memory logic and arithmetic operations. Although each technology faces specific challenges – lower density (MRAM, SRAM), endurance and variability issues (PCM, ReRAM, FeFET), and sequential accesses (RTM) –, they enable various in-memory functions such as bulk bitwise operations, and matrix-vector multiplication (MVM) [13], [18], [28], [32], [33], [38], [39], [52], [56], [61]. Memristive crossbar arrays have drawn particular attention for performing MVM via analog computation in theoretically $\mathcal{O}(1)$ time and with comparable performance to digital CMOS [53]. However, their widespread usage is hindered by reliability issues and costly digital-to-analog (DAC) and analog-to-digital (ADC) conversions. Despite advances in ADCs/DACs, crossbars suffer from high inaccuracy due to device variations and conductance drift, limiting their use to a few application domains [29], [53].

In contrast, DRAM and RTMs do not suffer from device non-linearities and offer unlimited endurance with inexpensive write operations, making them ideal for bulk-bitwise logic [2], [25], [32], [35], [39], [41], [49], [52], [61]. While the fault rate in RTMs increases in CIM-enabled designs, it is significantly less prevalent compared to memristors. For example, fault rates for DRAM- and RTM-based CIM range between 10^{-1} and 10^{-6} , compared to 10^{-1} in memristors [2], [39], [50], [52], [61]. On the other hand, in terms of performance, bitwise multiplications can be more expensive than their analog counterpart, exhibiting $\mathcal{O}(n^2)$ complexity [49]. Recent research for binary/ternary matrix multiplication, either involving power-of-two shifts [13], [39], [44], [63] or leveraging ternary weights networks (TWNs) [34], [37], have reduced complexity for bulk bitwise CIM. This is achieved by replacing multiplications with additions, which are implemented using majority gates in DRAM [18], [38]. However, for larger n -bit operands, the $\mathcal{O}(n)$ costs of the long carry chains remain prohibitively high for adder-based approaches.

In this paper, we introduce Count2Multiply, a novel approach to perform multiplications based on bulk-bitwise CIM using *high-radix massively parallel counting*. The high-radix counting reduces the operations needed compared to binary addition. Count2Multiply considers *accuracy as a first-class optimization metric*, incorporating a novel reliability scheme that protects all CIM operations. Unlike existing designs,

the Count2Multiply approach is technology-agnostic, which we demonstrate with implementations in DRAM and RTM. We leverage the counting to perform integer-binary and integer-integer matrix multiplications, a critical primitive in TWNs [34], transformer networks [37], and pre-alignment filtering [20].

Our contributions are as follows:

- We propose a high-radix in-memory counting methodology using digital in-memory operations (Sec. III).
- We illustrate how our in-memory counting mechanism, applied in different technologies, can be used to execute massively parallel integer-binary matrix multiplication, also extended to integer matrix-matrix multiplications through bit-slicing, in Sec. IV.
- We demonstrate how traditional row-level ECC can be extended to protect CIM operations in Count2Multiply, while still protecting row-level accesses (Sec. V).
- Finally, in Sec. VI, we evaluate Count2Multiply on multiple applications from the bioinformatics and machine learning domains and compare its performance and energy to state-of-the-art accelerators.

Our method improves performance by up to $10\times$, delivering $3.8\times$ higher GOPS/Watt, and $1.4\times$ higher GOPS/area with respect to the prior in-DRAM designs [18], [38].

II. BACKGROUND AND RELATED WORK

This section provides background on DRAM and RTM technologies, including their CIM capabilities, followed by an overview of the state-of-the-art digital CIM accelerators.

A. DRAM and compute-in-DRAM

A DRAM cell consists of a capacitor and a transistor (Fig. 1(c)), with cells organized into a 2D array of rows and columns. Each array is connected to a row of sense amplifiers (SA), also known as the row buffer. Reading or writing the values (capacitor states) of a particular row in the array involves a three-step process. First, the row is *activated*, bringing the data of that specific row to the row buffer. Second, the *read/write* operation transfers the data from/to the row buffer to/from the bus. Third, the row is *precharged*, restoring the bitlines to a stable state for the next operation.

Previous research has demonstrated that by carefully modifying the standard sequence of DRAM operations, certain tasks can be performed *in-memory*, without the data leaving the array [16], [51], [52]. For example, copying (row-cloning) the contents of a specific row *src* to another row *dst* in the same array can be achieved with back-to-back activations of the two rows followed by a precharge command, i.e., activate-activate-precharge (AAP). Activating the *src* row allows the SAs to strongly drive the row, bringing the *src* contents to the SAs and the bitlines. Subsequently, activating the *dst* row overdrives the capacitors in *dst* with the values on the bitlines [51]. Finally, a precharge command is issued to prepare the subarray for the next operation. The entire AAP operation takes around 49 ns [52], and is a fundamental primitive for in-DRAM computing.

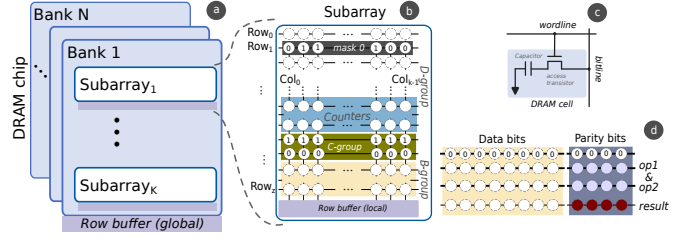


Fig. 1: Main memory (a) organization (b) subarray (c) cell and (d) CIM example invalidating traditional ECC parity.

In-DRAM computing leverages *multi-row activation*, wherein multiple rows in an array are activated *simultaneously* to implement logic operations. Numerous proposals demonstrate in-DRAM computing using charge-sharing [18], [52], [61] or by intentionally violating memory timing parameters [16], [64]. The Ambit’s scheme [52] is both simple and practical. It requires few changes to the DRAM array and has a well-defined set of instructions, while being less susceptible to CIM faults than schemes that require no changes. For this reason, we adopt Ambit to implement our in-memory counters.

Ambit relies on the fundamental concept that the simultaneous activation of three arbitrary rows – referred to as triple-row-activation (TRA) – results in a bulk bitwise *majority* function. This means that the final state of a bitline corresponds to the majority state of the three cells, a MAJ3 operation. Ambit exploits this principle to implement the logical AND and OR operations by setting one of the three rows to ‘0’ and ‘1’, respectively. To achieve functional completeness, a NOT operation is implemented using a special row of dual-contact cells (DCCs) [36]. In a DCC, one transistor connects the capacitor to the bitline, while another connects to the complementary bitline of the SA circuit [36], [52].

The TRA is destructive, as all activated rows are updated to the final state of the bitline. Most bulk bitwise operations use AAP operations for row-cloning the TRA result to *dst*, with occasional AP operations involving an activate followed by a precharge, taking one address as input. To simplify the row decoding logic, Ambit divides the space of row addresses in each subarray into three groups, as shown in Fig. 1(b): (i) B-group, a bitwise group of eight rows for bulk bitwise MAJ3/NOT operations, (ii) C-group, two control rows that store constants ‘0’ and ‘1’, and (iii) D-group, the remaining $r - 10$ rows for data storage, where r is the total number of rows per subarray. Like in previous works [52], [61] we assume the granularity of the CIM operation is mat-wise. So, in our case, each TRA operates on three rows of size 512.

B. Racetrack memory and in-RTM computing

Racetrack memory is a nonvolatile memory where each cell is a magnetic nanowire, or *track*, that can be divided into approximately 100 tiny magnetic regions called *domains*, with each domain representing a single data bit, as shown in Fig. 1(d). Accessing data in RTM involves *shifting* the desired bit to align it with an access port (AP) position, i.e., the fixed layer shown in dark blue. Extra padding domains (shown in orange) are required to prevent data loss during

shifts to the extremities. Similarly to other technologies, RTMs are organized into ranks, banks, and subarrays. Each subarray consists of a grid of *domain block clusters* [6] or DBCs which are groups of tracks (Fig. 8). We assume a subarray organization of 16 DBCs composed of 32-length tracks to total 512 rows per subarray.

Unlike DRAM, CIM in RTM is implemented using a special read operation [14], [48]. One such special operation is the *transverse read* (TR) that is performed on a region of a track, i.e., between two APs or between an AP and an extremity of the track, and returns the number of ones (or zeros) in that region [48]. Recently, CORUSCANT [39] leveraged the TR operation to propose multi-operand bulk bitwise logic and integer addition with two-operand multiplication. POD-RACING [41] extended this to floating-point addition and multiplication. To the best of our knowledge, HDCR is the only work that discusses counting in RTMs, and it does so with a limited scope [25].

C. Reliability schemes for CIM

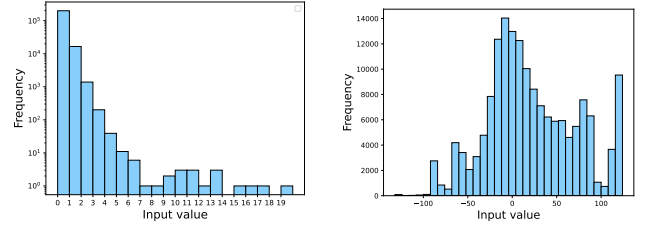
Most CIM systems typically leverage the charge- or current-sharing mechanism on the bitline of the memory array, which often leads to a higher chance of faults. Depending on the memory technology and the CIM operation type, the fault rate can be as high as 10^{-1} [64]. In the context of digital CIM, a fault is defined as a bit flip, where the obtained result is the inverse of the expected result.

For RTMs, a recent technique called CIRM-ECC promise protecting TR-based logic operations [8]. However, for CIM operations in DRAM, we are not aware of any ECC scheme and recent studies have reported fault rates as high as 10^{-1} – 10^{-4} [16], [52], [64]. Thus, for reliable CIM in DRAM, it is essential to develop solutions that protect against these faults.

Traditional ECC schemes employing parity bits cannot protect CIM operations of AND, OR, or MAJ. Fig. 1(d) illustrates a scenario where memory rows store data bits (green) with traditional valid ECC parity bits (blue). During these CIM operations, there is no current method to generate parity bits for the result, rendering the parity bits invalid (red). Thus, most CIM designs [33], [39], [52] provide no fault tolerance other than by replication and voting [39], [52]. The fault tolerant CIM designs [11] are not directly compatible with traditional memory ECC codes. In Section V, we propose a reliability scheme that leverages traditional ECC, like Hamming and BCH codes, to protect memory access and CIM operations in DRAM. Moreover, on-chip ECC parity checking supports the capability to do CIM ECC without sending the result to the memory controller.

D. Rationale of high-radix addition

Current state-of-the-art in-DRAM addition approaches, such as those based on ripple carry logic [13], [18], [32], suffer from long carry propagation chains, making them costly to be implemented with AAP/AP primitives. They are especially inefficient for memory-intensive applications like genomics and AI, which often involve accumulating low-precision inputs



(a) Short-read token repetition (b) 8-bit quantized BERT

Fig. 2: Input distribution in DNA pre-alignment filtering and BERT language model.

of 8 bits or less. Fig. 2 illustrates the input distributions of a DNA sequence alignment task and a quantized large language model. Ideally, the addition algorithm should exploit the narrow values when accumulating these inputs and result in a reduced input-dependent latency rather than the $\mathcal{O}(n)$ cost dominated by a wider accumulator width.

High-radix numbers offer a solution by mitigating latency and performance issues associated with sequential ripple carry by reducing the carry chain and requiring fewer addition stages, thereby improving the accumulation of large and small operands [4], [57]. In theory, addition in radix, or base, R has a carry chain of $\log_R(2^n)$ instead of n . Despite this, there is no efficient method for in-memory R -radix addition. This involves finding an appropriate encoding method, describing operations in terms of CIM primitives, and optimizing them for accumulating narrow values. With our proposed in-memory counting, we address these issues as explained next.

III. IN-MEMORY HIGH-RADIX COUNTING

This section describes our technology-agnostic in-memory counting technique using high-radix counters. We use *Johnson Counters* (JCs) as their encoding lends itself to efficient realization in DRAM and other memory technologies that can implement bulk-bitwise CIM operations. For future sections, we assume a conventional main memory organization having ranks, banks, and subarrays. Each subarray has a local row buffer, while the global row buffer is shared between the subarrays within a bank (Fig. 1(a)).

A. Core counter design

Let us consider a single-digit n -bit JC that can count from 0 to $2n - 1$, i.e., radix- $2n$. For instance, $n = 5$ corresponds to a single-digit base-10 counter, from 0 (“00000”) to 9 (“00001”). Our n -bit JC implementation requires $n + 4$ memory rows wherein each column stores an independent counter. The four overhead rows store temporary values for intermediate results.

1) *Single-digit unit increment*: Fig. 3 illustrates an example of C JCs, with the overhead rows and bit positions, i.e., most significant bits (MSBs) and least significant bits (LSBs), labeled on the right. To increment all C counters, all bit positions “promoted” (shifted) by one towards the MSB. The LSB is formed by back filling with the inverse of MSB (MSB), effectively a form of *inverted feedback*. To achieve this with CIM, the MSB is initially cloned into an overhead

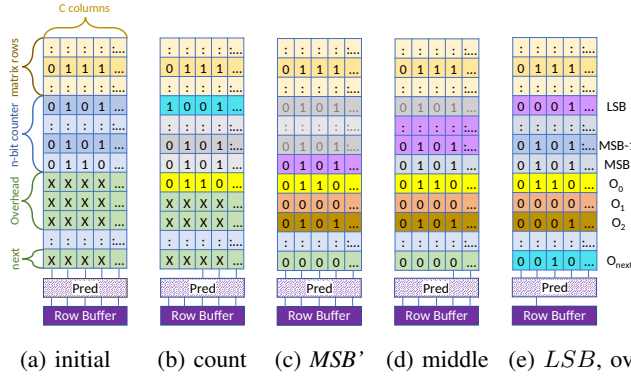


Fig. 3: C , n -bit Johnson counters, in memory: (a) before counting; (b) all counters count; (c)–(e) masked counting.

position, e.g., O_0 . Subsequently, all bits of the counter are shifted (copied) by one position towards higher significance. The *forward shifts* are implemented with a series of row clones (RCs) while the *inverted feedback* is implemented with RC and NOT operations (see Sec. II-A).

Consider the initial counters state in Fig. 3a. First, the MSB row is copied to O_0 , i.e., $O_0 \leftarrow \text{"0110..."}$. In DRAM, this counter *setup* requires a single AAP operation. Subsequently, $(\text{MSB}, \dots, (\text{LSB}+1)) \leftarrow ((\text{MSB}-1), \dots, \text{LSB})$, respectively, as shown in gray in Fig. 3b. Finally, the inverted O_0 is copied into the LSB, i.e., $\text{LSB} \leftarrow \overline{O_0}$ shown as $\text{LSB} \leftarrow \text{"1001..."}$. Compared to the initial state of the four counters in Fig. 3a, from left to right, the C counters in Fig. 3b are incremented as follows: $\text{"00...0"} \rightarrow \text{"00...1"} (0 \rightarrow 1)$, $\text{"11...1"} \rightarrow \text{"11...0"} (n \rightarrow n+1)$, $\text{"10...0"} \rightarrow \text{"00...0"} (2n-1 \rightarrow 0)$, and $\text{"01...1"} \rightarrow \text{"11...1"} (n-1 \rightarrow n)$.

2) *Masked unit increment*: In *masked counting*, only certain counters are updated, while others retain their previous states. To support this, we store a mask m in a row within the subarray containing the counters. Considering the initial state in Fig. 3a, let us assume the matrix rows (in tan) store the mask values ("0111..." for the running example). The counting process starts by copying $O_0 \leftarrow \text{MSB}$. In masked counting, only the counters with the mask bit set are shifted.

To implement the masked *forward shift*, the new MSB (MSB') must be constructed from a portion of the MSB (where $m_c = 0$ for bit in column c) and $\text{MSB}-1$ (where $m_c = 1$). The increment proceeds as follows: $O_1 \leftarrow (\overline{m} \text{ AND MSB})$; $O_2 \leftarrow (m \text{ AND MSB}-1)$. For our running example in Fig. 3c, $O_1 \leftarrow \text{"0000..."}$ = "1000..." AND "0110..." and $O_2 \leftarrow \text{"0101..."}$ = "0111..." AND "0101..." . Thus, $\text{MSB}' \leftarrow O_1 \text{ OR } O_2$, and from the example $\text{MSB}' \leftarrow \text{"0101"} = \text{"0000..."}$ OR "0101..." . This step must be performed on all remaining counter bits, i.e., $(\text{MSB}-1)' \dots (\text{LSB}+1)'$ which in this example stores "0101..." in each row, as shown in Fig. 3d. Then, we construct the *inverted feedback* as follows: $\text{LSB}' \leftarrow \text{LSB AND } \overline{m} \text{ OR } O_0 \text{ AND } m$, which is shown as $\text{LSB}' \leftarrow \text{"0001..."}$ = "0000..." OR "0001..." , in Fig. 3e. We refer to this process of updating the counter as *build row*.

Recall we are presuming the Ambit scheme [52] which

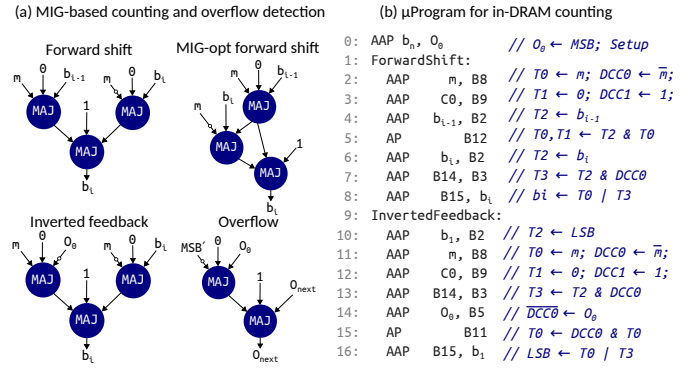


Fig. 4: Majority-based in-DRAM operations for counting and overflow detection¹.

reserves a set of rows called the “B-group” where CIM operations are conducted and the “C-group” where control rows, C_0 and C_1 . Using the control rows we can construct AND and OR from the MAJ3 function. To implement build row, we first synthesize the expressions into Majority-Inverter Graphs (MIGs) [3], as illustrated in Fig. 4(a). We further employ MIG-based optimizations, similar to those in SIMDAM [18], to minimize the number of rowclones needed for operations with C_0 in both forward shift and inverted feedback. By carefully scheduling the MAJ3 operations and allocating the B-group’s rows, we generate a μ Program of memory commands, e.g., AAP, to increment the counter. Fig. 4(b) presents the sequence of 7 AP/AAP primitives taken by each step of build row. Using AAP operations, the mask row m , C_0 , and the counter bit b_{i-1} are cloned to three rows in the B-group (Line 2–4 in Fig. 4(b)) and then MAJ3 is used to implement AND (Lines 5,7) and OR (Line 8) operations. The NOT operation is inherently handled by an rowclone operation with special DCC rows [52], so obtaining \overline{m} incurs no additional overhead. This process repeats for all n bits in the counter ($n-1$ forward shifts and one inverted feedback), resulting in a total of $7n$ operations, as summarized in Table I.

3) *Overflow detection and digit rippling*: For multi-digit counters, when the current counter rolls over (*overflows*) the next higher digit must be incremented. An overflow is detected when the MSB transitions from ‘1’ to ‘0’, i.e., when MSB AND MSB' is 1. A detected overflow in the least significant *digit* (LSD) generates a carry (O_{next}) to the next significant *digit*, which may ripple through to the MSD, depending on the state.

In masked counting, each increment can potentially cause an overflow in one of the counters. A naive implementation would fully resolve detected overflows in the LSD, propagating carries through all digits before proceeding to the next increment. This is inefficient because an overflow check after every increment is unnecessary, especially for unit and small value increments, limiting performance. To optimize this critical path operation, we introduce a dedicated overflow row, O_{next} , in memory. After every build row, we compute $O_{\text{next}} \leftarrow O_{\text{next}} \text{ OR } O_0 \text{ AND MSB}'$ for detecting a potential

¹We modified Ambit’s B-group mapping [52] so address B11 activates T_0 , T_1 , and DCC0 . This does not affect prior operations as B11 was unused.

TABLE I: CIM operations required for one masked increment.

Tech.	DRAM [61]		RTM [39]	
Op.	base	pred	base	pred
Setup	1	1	5	0
Build row	7n	2n	17n	2
Overflow	6	6	8	1
Total $f(n)$	7n+7	2n+7	17n+13	3

overflow in the LSD, and continue with the next increment. Calculating O_{next} , as illustrated in Fig. 4 (a, majority-based overflow), requires a total of six AAP operations (Table I). The increment due to the carry in the next significant digit(s) is delayed until it is unavoidable – before a second overflow occurs. This approach leverages the fact that unit increments can never cause two overflows in the same digit within a span of $2n$ increments. This significantly reduces the number of CIM operations not only for unit increments but also for small value increments, as discussed in Section III-B1.

For negative inputs, the counter can decrement through *backward shifts* and *inverted feedback* during build row. The *underflow* detection mechanism is similar to overflow except the MSB transitioning from zero to one and the O_{next} bit is used to decrement the next significant digit accordingly. Overflows or underflows must be resolved before switching from increment to decrement and vice versa, or a row representing a sign-bit of overflow must be allocated, O_{sign} .

4) *Multi-digit masked unit increment*: For d -digit counters, all digits are stored in the same column, requiring $d \cdot n + 4$ rows, and updated sequentially using the single-digit counting mechanism. After $2n$ increments (*build row* and *overflow detection*) to the *LSD*, O_{next} is used to increment the *LSD*+1 and subsequent digits through O_{next} rippling. For counter addition, i.e., adding a multi-digit input to a multi-digit counter, we align digits with equal significance and update all digits sequentially from the LSD, resolving carries as we move to the MSD. The increment process is repeated $s + d$ times, where s is the digit sum of a number in the base $2n$. This sequential digit increment is expensive, requiring $(s+d) \times f(n)$ CIM operations. In the next section, we propose a series of optimizations to reduce the number of CIM operations.

B. Optimized counters design

The number of CIM operations in Table I are for a unary increment in a single digit of the Johnson counter. In practice, inputs may have multiple digits, and increment values between one and $2n - 1$, increasing cost proportional to the values and number of digits. While modifying the Ambit design (e.g., by increasing rows in the B-group) could improve performance, we keep the baseline design unchanged and propose scheduling optimizations to improve counters' performance.

1) *Variable-step (k -ary) increment*: This section presents an optimization to perform an increment by k , where $1 \leq k \leq 2n - 1$ with the same number of steps as a unit increment. For all cases, the number of shifts (row clones) is equal to the number of counter bits (n) but varies in pattern such that k -ary counting shifts all the bits by k steps and changes the number of forward shifts and inverted feedback steps. Fig. 5,

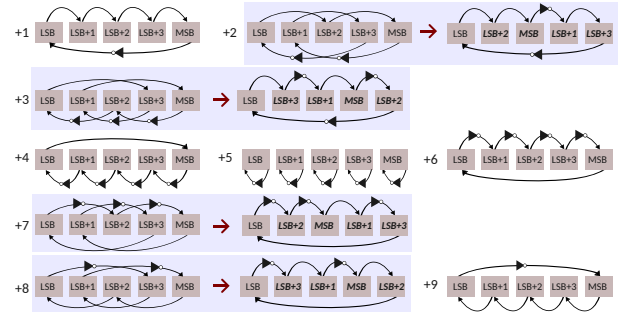


Fig. 5: Shifting patterns of a 5-bit counter for incrementing any value between 1 and 9.

which illustrates k -ary counting for radix-10 counting, shows the process requires the same number of fundamental steps operations for any k . We observed that the value of k only changes how many NOT operations are required. Fortunately, NOT does not require any additional CIM operations and does not affect performance.

Algorithm 1 demonstrates how counter bits are updated based on k . If k is less than or equal to n , Lines 2-7 conditionally update the counter state using a mask m , and calculate the digit overflow, as shown for increments 1 to 5 in Fig. 5. Line 4 corresponds to the upper arrows, while Line 6 represents the lower arrows with a NOT operation. For increments 6 to 9, Line 11 corresponds to the upper arrows, and Line 13 represents the arrows with a NOT operation.

Fig. 6a compares the average number of AAP operations required for different bases when accumulating 8-bit inputs on counters with 16, 32, and 64 bits capacities. A d -digits counter with n -bits per digit has a capacity of $(2n)^d - 1$. k -ary counting provides a 2–6 \times reduction in CIM operations over unary counting for varying-radix counters.

Algorithm 1: Variable-step increment for n -bit JC

Input: Johnson counter $C \leftarrow [b_1, \dots, b_n]$, mask m , increment amount k

```

1 if  $k \leq n$  then
2   for  $b_i$  from  $\{C_{n-j} \mid j \in [0, n-k]\}$  do
3      $b'_i \leftarrow (\overline{m} \wedge b_i) \vee (m \wedge b_{i-k})$ ;
4   for  $b_i$  from  $\{C_j \mid j \in [1, k]\}$  do
5      $b'_i \leftarrow (\overline{m} \wedge b_i) \vee (m \wedge \overline{b_{n-k+i}})$ ;
6    $O'_{next} \leftarrow O_{next} \vee (b_{n-1} \wedge \overline{b'_{n-1}})$ ;
7 else
8    $k \leftarrow k - n$ ;
9   for  $b_i$  from  $\{C_{n-j} \mid j \in [0, n-k]\}$  do
10     $b'_i \leftarrow (\overline{m} \wedge b_i) \vee (m \wedge \overline{b_{i-k}})$ ;
11  for  $b_i$  from  $\{C_j \mid j \in [1, k]\}$  do
12     $b'_i \leftarrow (\overline{m} \wedge b_i) \vee (m \wedge \overline{b_{n-k+i}})$ ;
13   $O'_{next} \leftarrow O_{next} \vee (b_{n-1} \vee \overline{b'_{n-1}}) \wedge m$ ;

```

2) *Run-time overflow minimization*: With k -ary counting, each count would require $2z \times f(n)$, where z represents the input digits. However, it is possible to delay outstanding overflows. Essentially, O_{next} for each digit provides enough storage to represent $4n - 1$ values, which can be used to identify when it is necessary to ripple O_{next} . $O_{next} = 1$ represents $2n$ for the current digit or 1 for the next higher digit. Fig. 7 illustrates how accumulating an input with fewer than d

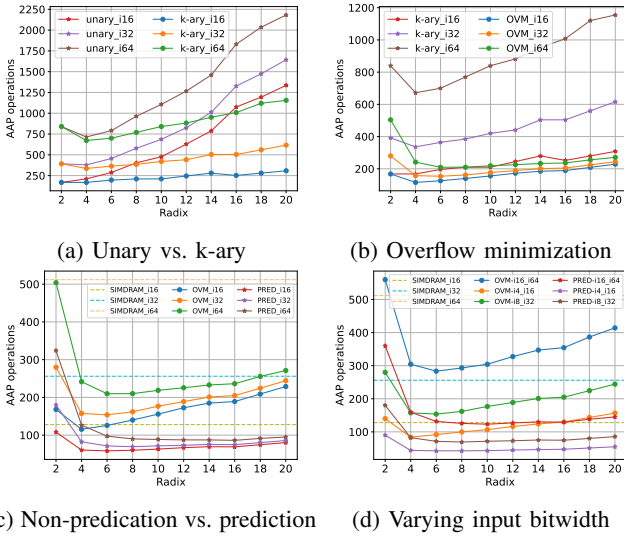


Fig. 6: Performance comparison between unary, k-ary, overflow minimization, predication and ripple-carry logic [18].

digits, i.e., $z < d$, effectively delays the propagation of O_{next} . When the LSD overflows and ripples to $LSD + 1$, the counter, even if all digits are at their maximum value $(2n - 1)$, can still increment $2n$ more times before another overflow occurs for $LSD + 1$.

The olive boxes in Fig. 7 show outstanding overflows and the final state shows the counter values after overflow resolution. In the top row of the figure, there were ten increment-by-nine commands issued. Regardless of the initial counter value or mask pattern, we know we can increment at least ten ($2n$) single-digit values by rippling up to only one additional digit, $LSD + 1$, before handling overflow at the next, or $LSD + 2$. Essentially, the olive squares are storing 14 and 18. The bottom example of Fig. 7 shows for 2-digit values, at least $2n$ values can be accumulated in the three lowest-order digits before rippling through higher-order digits as needed. This assumes all mask bits are 1, providing a safe margin.

As increment values are broadcast by the memory controller to the counters, the MC can track the worst-case overflow requirement (presuming m was always true for at least one counter) and issue overflow commands as necessary to guarantee correct execution while minimizing overflow steps. Unlike CIM adders where the cost is determined by the maximum value, the cost of counting is input dependent. To demonstrate the impact of increment value on the increment cost, Fig. 6b shows the average number of AAP operations required for various radices when accumulating 8-bit inputs on counters capable storing values of $\geq 2^{16}$, $\geq 2^{32}$, $\geq 2^{64}$. For use cases where the input is limited to small values, e.g., 8-bit or fewer (see Sec. II-D), the frequency of overflow is significantly reduced, leading to improved counter performance.

3) *Predicated in-DRAM counting*: Masking and combining rows, the most frequent CIM operations in JC's, can be eliminated by introducing additional bit-level masking hardware. Hardware masking is already common in DRAMs at

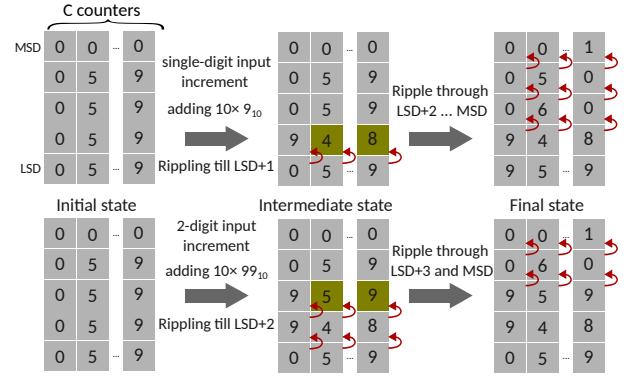


Fig. 7: Incrementation with delayed overflow resolution.

the byte-level [10], [42]. The increment operations are then only performed in columns where the predication hardware is driven by the mask. This results in a build row latency of only $2n$ cycles compared to $7n$ in non-predicated counting.

The predication circuitry latches the mask into the data-in register used for writing, and all columns are set to an equilibrium state of $VDD/2$ (precharged). Multiplexers controlled by the mask connect each column to either the row buffer or a high-impedance state. Finally, a row-clone is performed as in Ambit [52], but the columns that we do not want to overwrite remain connected to a high-impedance state and are thus unaffected. This is essentially equivalent to the hardware overhead of differential write in NVMs [9], [62].

Fig. 6c compares pred and non-pred counting with SIMD-RAM [18] in terms of AAP operations. The figure considers k -ary increments with overflow optimizations and uses 8-bit input following a uniform distribution. Even without predication, JC's (base > 2), particularly for larger capacity counters dramatically improve over SIMD-RAM. The predicated counters reduce the CIM operations by almost another $2\times$.

4) *Impact of input range*: Fig. 6d illustrates the impact of the input bitwidth (4, 8 and 16-bit integer inputs) on the counter performance retaining significant improvements over SIMD-RAM and a good improvement from predication [18].

C. Counting using other memory technologies

The bulk bitwise counter concept, e.g., using (MAJ, AND, OR, NOT), is technology-agnostic and applicable to many CIM concepts. We demonstrate its implementation an NVM particularly suited to predication and generalize to other NVMs.

1) *In-RTM counting*: CORUSCANT (see Sec. II-B) requires two access ports AP_0 and AP_1 as shown in Fig. 8. During setup, MSB is copied (using a mechanism similar to rowclone) to AP_1 of DBC_{i+1} and then shifted twice below AP_1 , DBC_{i+1} where i is the DBC that stores the counter. Next, \bar{m} is copied to AP_1 of DBC_{i+1} after being read using the NOT operation, which takes one cycle. Then, \bar{m} is shifted once below AP_1 . Finally, m is copied to AP_0 . This setup enables us to rapidly switch between masking operations with m and \bar{m} when updating the counter. Overall, this setup requires seven operations (copy, shift, shift, NOT, write, shift, copy). Updating the counter requires sending a copy of each next row and using

either end of the processing region (between AP_0 and AP_1) to conduct the AND operations. This requires the extra rows are reset to “0...0.” Computing the OR requires setting the extra rows to “1...1.” This requires extra writes, or as described in CORUSCANT, shifts between the preset and reset regions. Due to the significant shifting, building rows with a single processing region takes $17n$ cycles (Table I). Similarly, the overflow calculation requires another 8 cycles.

The RTM counter can be improved by adding additional processing regions for each unique operation. With separate processing regions for performing AND and OR operations, building rows takes only $7n + 3$ cycles. Since one AND always takes m as an operand and one always takes \bar{m} as an operand we can reduce the build row latency to $5n + 3$ cycles by adding an additional AND region. The overflow operation can benefit from a similar reduction in shifts by allotting another processing region, reducing the cycle count to 5. Each additional processing region requires $d = 5$ rows, meaning our most performant setup requires 20 additional rows – $4\times$ the memory required for each counter digit.

Still, an additional performance overhead of n cycles is incurred for rippling the count beyond a single digit. The n shifts are needed to shift the access port to the next digit. Therefore, computing with CORUSCANT is not efficient for in-memory counting because it is not leveraging the natural shifting, suggesting predicated counting.

2) *Predicated counting*: For predicated counting in RTMs, we propose an extension to the RTM circuit shown in Fig. 8(a) for a single nanowire that implements a radix-10 JC. The access ports are placed $d = 5$ domains apart. To *write and shift* a section of the nanowire can be accomplished using a technique called *transverse writing* [40]. To write and shift in a ‘1’ would require turning on $WWL_{0,1}$ and $WWL_{1,0}$, shifting a ‘1’ into AP_0 while shifting towards AP_1 , with the value stored at AP_1 shifting out. Thus, by reading the value at AP_1 , its inverse can be shifted into AP_0 using this approach.

In Fig. 8(a), we add a *pred* transistor in parallel with $RWL_{1,1}$. This works by replacing the $WWL_{1,x}$ connection with a current sink to GND through *pred*. If *pred* is ‘1’ the TW exits to GND and the counter advances. Otherwise, there is no path TW current path and the counter does not advance. This additional transistor decreases the build row cycle count from $17n$ to 2.

For in-memory counting, we can replace the CORUSCANT logic circuitry with a single predication buffer, which is a significant savings. We also added a dedicated overflow detection circuit, built from flip-flops. Prior to counting, the overflow circuit is reset to “0...0” using an asynchronous *reset* input. During counting, the accumulator “rolls over” when the MSB transitions from ‘1’ \rightarrow ‘0’ allowing \overline{BL} to trigger that bit of the overflow circuit to store a ‘1’. This occurs in base 10 if the counter increments from ‘9’ \rightarrow ‘0’. This can save the setup and overflow detection cycles.

3) *Extension to other technologies*: This approach for building JCs in memory is extensible to other CIM approaches, even if they use different bulk bitwise instruction sets. For instance, MAGIC [28], [56] offers single-cycle NOR operations,

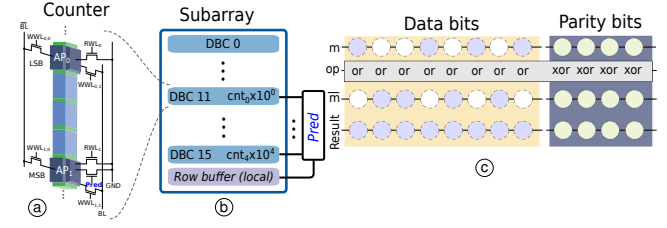


Fig. 8: Overview of RTM-CIM (a) Predicated counter device/circuit, (b) subarray predication architecture, (c) CIM of two masked rows maintaining ECC

which be mapped to OR ($\overline{A + B} \rightarrow$ inversion) and AND (three NOR steps) such that build row requires $8n + 1$ cycles and overflow takes 5 steps, two for the OR and three for the AND. Predicated counting is similar to DRAM.

IV. COUNT2MULTIPLY

This section introduces Count2Multiply, leveraging our counting technique from Section III, for both integer-vector binary-matrix (IVBM) and fixed-point matrix multiplication.

A. Integer-vector binary-matrix (IVBM) multiplication

Binary matrix multiplication is fundamental various applications, including integer factorization [23], spectral graph theory [5], neural networks [46], and context-free grammar recognition [30]. In neural networks, using real-valued inputs and binary weights offers an optimal trade-off on resource-constrained devices [22], [46]. In-memory IVBM nearly eliminates weight data movement and can be efficiently implemented using in-memory counters.

Let us assume that the input vector v consists of x base- $2n$ integers. To compute $v \cdot B$, where B is a $x \times z$ binary matrix, counters are iteratively incremented by position value for each base- $2n$ value from vector v of size x . When adopting conservative bank-level parallelism (BLP), incrementation occurs digit-wise, with all d digits of a counter stored in the same column within a subarray. This process requires $\sum_{i=1}^x ([\log_{2n}(v_i)] + 1) \times f(n)$ cycles, $f(n)$ from Table I and an additional rippling overhead when increments cannot be guaranteed not to exceed $2n$.

Tiling matrix B depends on the memory array size and BLP. To effectively leverage BLP in large matrices, we distribute B 's rows across pb simultaneously activatable banks, operating them in parallel with distinct segments of vector v . Each bank is assigned a subset of the matrix's rows (i.e., x/pb rows) along with a partial counter. To obtain the final output, we sum partial counters by transferring counters between banks using pipelined serial mode rowclone [51] and, then, adding pairs of counters with Algorithm 2. This scheme eliminates inter-bank copying of matrix B rows. Only the counter's $d \cdot n$ rows are transferred between subarrays, reducing data movement and enabling scalable counting across the entire matrix

B. Fixed-point matrix multiplication

Many machine learning and robotics applications use 2-16 bit floating-point precision [17], [21], [37], [47]. Handling

Algorithm 2: Johnson counter addition

Input: Counters C_1, C_2

```

1  $O_3 \leftarrow C_2.MSB$ ;
2 for  $b$  in  $[C_2.MSB, \dots, C_2.LSB]$  do
3    $mask \leftarrow b \vee O_3$ ;
4    $\text{increment}(1, C_1, mask)$ ;
5  $O_3 \leftarrow mask$ ;
6 for  $b$  in  $[C_2.LSB, \dots, C_2.MSB]$  do
7    $mask \leftarrow \neg b \wedge O_3$ ;
8    $\text{increment}(1, C_1, mask)$ ;

```

real-valued inputs as fixed-point numbers is relatively common, with p bits of precision. Implementing this in fixed-point with Count2Multiply requires converting the second matrix into binary, conducting multiple integer-matrix binary-matrix multiplications (IMBM), and subsequently aggregating the results using shift and add operations. For instance, when computing $A \cdot B$, where A is a p -bit fixed-point input matrix and B is an unpacked p -bit fixed-point matrix as $C = \sum_{i=0}^p 2^i (A \cdot B^i)$.

For FPM, we transform the integer matrix B into $2 \times (p-1)$ power-of-two equivalent binary matrices. This transforms a 2D matrix (B) into a 3D matrix (B_{bit}), whose last dimension is $2 \times (p)$ and is readily an IMBM operation. This representation also exploits the inherent BLP but requires a compulsory accumulation step, i.e., a shift-and-add operation. In our case, it requires adding JCs to JCs and the left-shift operation which are also implemented using our counters, as explained next.

C. Other operations using high-radix counters

Counter addition:

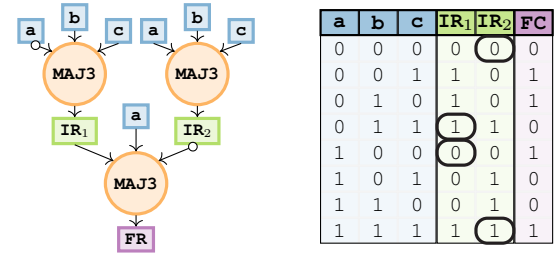
Using the counter state as input for counting is slightly different from using the base-2n input described in Section IV-A. This approach, detailed in Algorithm 2, involves sweeping one of the n -bit counters (C_2) twice to generate masks that are used to increment a second counter (C_1) in place, i.e., $C_1 \leftarrow C_1 + C_2$.

Counter left-shift The operation $c \ll i$ can be achieved by successively adding the counter value to itself i times, which effectively doubles the counter's value with each iteration, corresponding to the multiplication by a power of two.

ReLU Performing the ReLU function with high radix values involves similar principles to those in a standard binary system, that is, checking if the number is non-negative. As we represent negative ranges with a separate underflow bit, if the underflow bit is one, then we set the output to zero. Otherwise, the output remains the same as the input. This is done by ANDing all b_i values with the $\overline{O_{sign}}$.

V. FAULT TOLERANCE FOR IN-MEMORY COUNTERS

High fault rates in CIM operations, especially in DRAM, require a protection scheme (Section II-C). For RTM, we employ CIRM-ECC [8] to protect CIM operations. For DRAM, we propose a general scheme applicable to *any* TRA operation and demonstrate it with in-memory counters (Section III).



(a) Majority-inverter graph [3] (b) Truth table with unlikely faults circled

Fig. 9: Synthesis of XOR function via MAJ3 gates

A. Fault protection scheme setup

ECC codes are typically not homomorphic over AND or OR operations. However, many commercially used ECC codes, including Hamming codes, Reed-Solomon, and BCH codes, are homomorphic over XOR. We wrap our CIM operations in XOR to enable the use of traditional ECC codes for them. The synthesis of an XOR gate using MAJ3, i.e., TRA operations (see Sec. II-A), is a two step process, as shown in Fig. 9a. The two intermediate MAJ3 gates produce IR₁ and IR₂, that generates the XOR result to fault check, FC. The fault rate in majority gates themselves exhibit a data-dependent pattern, i.e., when the majority gate is operating on all '1's or all '0's, a fault is much less likely than a read fault. This impact on XOR synthesis is highlighted in Fig. 9b. We assume homogeneous '0' or '1' cases exhibit the read access fault rate.

Fig. 9b tabulates the values of IRs and FC for all possible inputs. Nearly all potential faults in either the IRs or the FC lead to an invalid parity check, detectable using standard ECC. The combinations in which a fault does not alter the FC value are circled in the figure. Note that all possible undetectable faults are these homogeneous input cases. Thus, the scheme can detect all critical single-gate faults in IR₁ or IR₂. Additionally, in cases where both IR₁ and IR₂ could fault, the corresponding value in FC will also flip, making the faults detectable via the parity check. Therefore, the only undetectable faults occur when one of the IRs faults *and* the FC also faults.

This single error detection scheme can be extended to double and triple error detection, or further by repeating the computation of FC. If any of the computed FCs fail the ECC check, the computation is repeated from the beginning with a, b , and c , generating new IRs and FC in the process.

B. Integrating fault tolerance with in-memory counting

In our counting technique, we build each new row by combining two rows (positions i and $i-k$) masked with m and \bar{m} . Here, a traditional OR operation acts as an XOR, presuming an XOR for the parity bits [65], as shown in Fig. 8c. This is because masked (white) locations are set to '0', so '1's can only be stored in unmasked (gray) locations, ensuring that '1's are mutually exclusive between the two rows. However, this method only works once the masked rows are created. Fig. 10 provides an example of protecting the critical masking step: a

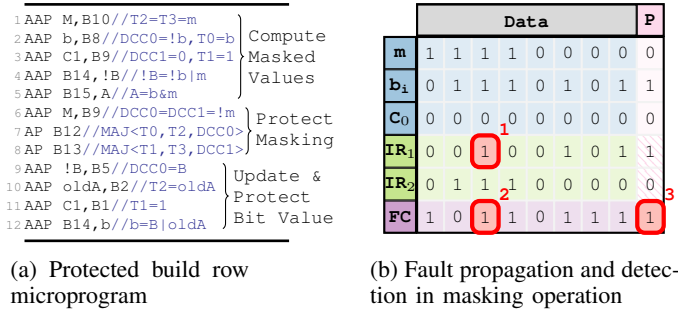


Fig. 10: ECC scheme for in-memory counting

fault in IR₁ causes the final parity check to fail, signaling a fault that requires repeating the computation.

For protected-counting, we change the Ambit address grouping by rewiring address B11 from T0, T3 to $\overline{DCC0}$, $\overline{DCC1}$; address B12 from T0, T1, T2 to $\overline{DCC0}$, T0, T2; and address B13 from T1, T2, T3 to $\overline{DCC1}$, T1, T3. Note that this does not affect the row decoder or the size of the groups. Listing 10a details the build row operations with these new address groups when using our protection scheme. This build row step includes computing the masked values (lines 1-5) and protecting the masking step (lines 6-9) which demonstrate how additional operations can enable traditional ECC checks to detect errors in AND results.

Note, the new order of computations in our protected build row. Previously, we computed b_i AND \overline{m} and b_{i-k} AND m together in one build row step. Here we compute b_i AND \overline{m} and b_i AND m in one build row step to do the protection, while trusting that b_{i-k} AND m has been computed and protected previously. In the subsequent build row step, we use the b_i AND m result, so only one additional temporary row is required for this optimization.

Fig. 10b shows how a fault in the masking step can be protected by our scheme. First, we compute the values: the majority result of mask m , counter bits b_i , and constant zeros c_0 constructs masked rows in IR₁ and IR₂. Then we check if there are any errors: in this case the fault in IR₁ (1) propagates to FC (2) causing parity check to fail (3). Once all necessary masked rows are created, they are ORed to update the current counter bit. This is equivalent to XOR and easily protected, as explained earlier. Once the masked rows are ORed, i.e., the build row step is completed, the next step is to check and update the overflow bit. For each overflow CIM operation, two additional MAJ3 steps are required because we cannot use both the IR₁ and IR₂ results in our counting process, so we need an extra IR and FC step. However, this cost is amortized since the overflow computation occurs only once per increment, while the build row occurs n times.

C. Beyond single fault protection ($\geq 2ECC$)

While the single error detection scheme can effectively square the probability of an undetectable fault, this may not suffice for higher fault rates, i.e., $10^{-1} - 10^{-4}$. Our protection scheme can be extended to two error detection and beyond. The number of times we repeat the FC is configurable. Further

modifying the address grouping (rewiring address B1 from T1 to T0, T1 we compute two additional FC operations with each repeat. Table II compares protection schemes with varying repeats applied to different inherent per-operation fault rates. The error rate and detect rate report the per-bit probability of an undetectable error and detectable error, respectively.

TABLE II: Effects of varying number of repeats for FC calculation on different inherent fault rates

Repeats	1			2			3		
Fault rate	10^{-1}	10^{-2}	10^{-4}	10^{-1}	10^{-2}	10^{-4}	10^{-1}	10^{-2}	10^{-4}
Error rate	1.4E-3	1.5E-6	1.5E-12	1.4E-5	1.5E-10	1.5E-20	1.4E-7	1.5E-14	1.5E-28
Detect rate	3.1E-1	3.5E-2	3.5E-4	4.4E-1	5.4E-2	5.5E-4	5.5E-1	7.3E-2	7.5E-4
Operations	$13n + 16$			$23n + 26$			$33n + 36$		

VI. EXPERIMENTAL SETUP AND RESULTS

Count2Multiply is simulated by extending NVMain/RT-Sim [24], [45] with a cycle-level CIM simulation model. Our implementation of Ambit and SIMDRAM in NVMain was rigorously validated against the results reported in [18], [52] and by MIMDRAM's simulator [38]. The DRAM- and RTM-based Count2Multiply are built on Ambit and CORUS-CANT [39], respectively. We compare our accelerator to a high-end GPU and a state-of-the-art in-DRAM design [18]. The architectural parameters of the memory organization are listed in Table III. The energy and latency parameters are the same as in the baseline CIM systems [18], [39]. Furthermore, our setup follows the organization and timing constraints of commercially available DRAM, including critical parameters affecting parallelism, e.g., tFAW and tRRD. Subarray-level parallelism is not considered.

A. Evaluated systems

We compare Count2Multiply across technologies with state-of-the-art in-memory adders and a GPU as follows:

- *SIMDRAM:X* State-of-the-art in-DRAM ripple carry adder [18] using X banks.
- *GPU*: NVIDIA RTX 3090 running GEMVs and GEMMs with ternary matrices using BitBLAS [58]. Each data point is the average of ten runs with a warm-up phase to avoid cold cache effects. GPU kernel performance and power reported with cudaEvents API and nvidia-smi, excluding data transfer. GPU area is 628 mm^2 [12].
- *C2M:X* refers to the non-predicated Count2Multiply, while its predicated counterpart is *PC2M*.
- *RTM-C2M:X* RTM-based Count2Multiply using X banks, predicated configuration is *RTM-PC2M*.

TABLE III: Memory organization and architectural parameters

DRAM	Memory Controller 8 kB row size, FR-FCFS scheduling Main Memory DDR4-2400, 1 channel, 1 rank, 8 devices + ECC DRAM chip 16 banks, 1 kB row size, 1024 rows per subarray
RTM	8 GB, 64 banks, 512 subarrays per bank Rows and columns per subarray: 512, 4096

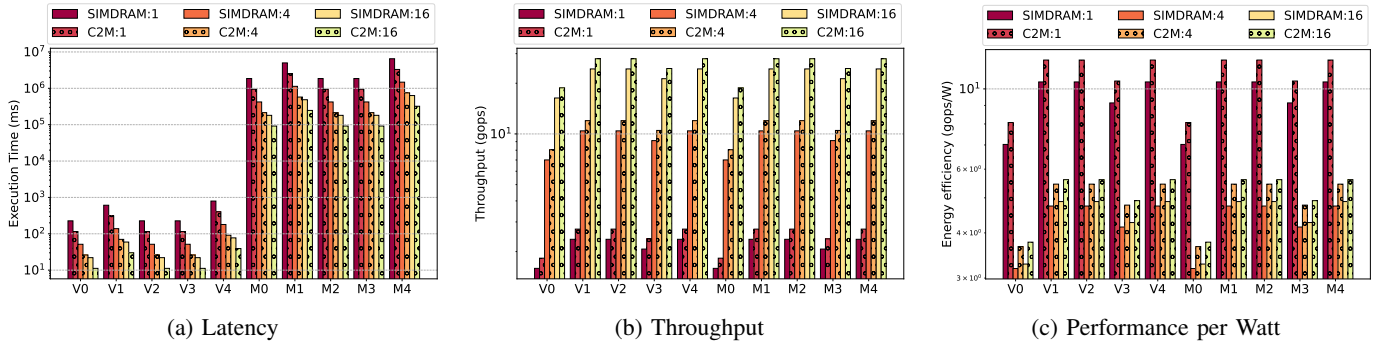


Fig. 11: Comparison of DRAM designs on ternary GEMV/GEMM from LLAMA and LLAMA-2 models [37], [54], [55]

TABLE IV: GEMV and GEMM dimensions from [54], [55]

Model	ID	M	N	K	ID	M	N	K
LLaMA	V0	1	22016	8192	M0	8192	22016	8192
LLaMA	V1	1	8192	22016	M1	8192	8192	22016
LLaMA-2	V2	1	8192	8192	M2	8192	8192	8192
LLaMA-2	V3	1	28672	8192	M3	8192	28672	8192
LLaMA-2	V4	1	8192	28672	M4	8192	8192	28672

B. Evaluated workloads

1) *GEMV and GEMM*: We use the GEMM and GEMV shapes (M, N, and K) from Table IV derived from the LLAMA and LLAMA-2 models [54], [55]. These shapes represent the key computational loads in the models and serve as effective proxies for assessing their performance.

2) *TWNs*: Convolutional layers are computationally most intensive in modern NNs. In our experiments, we consider three models: LeNet, VGG-13, and VGG-16.

3) *Transformer networks*: The attention mechanism faces memory-bound challenges due to its large-scale data requirements. We evaluate all GEMM operations in the attention layer of the BERT model as they are the most time-consuming component. Ternary parameters are also considered [37].

4) *Pre-alignment filtering*: Pre-alignment filtering is a memory-intensive step in DNA analysis pipelines, where the input genome is compared to a reference genome stored as bitvectors in memory [27]. Nucleotide pattern repetitions in the input genome are represented as integers. For our evaluation, we use a human genome and a similar setup to prior work [20].

C. Comparison to state-of-the-art CIM-DRAM

Fig. 11 presents a comparative analysis of the performance, i.e., latency, throughput and throughput per Watt, of only in-DRAM implementations for integer-ternary GEMV and GEMM workloads, as described in Table IV. The evaluation uses an 8-bit signed integer input and a radix-8 for the counter configurations. All configurations assume an accumulation capacity of 64-bit integers to ensure computational precision.

Due to the sequential nature of ripple carry in *SIMDRAM*, *C2M* consistently outperforms *SIMDRAM* on all workloads and all system configurations. On average (geomean), *C2M* is $2\times$ faster and delivers $1.15\times$ higher throughput and throughput per Watt. This finding is in agreement with previous results obtained for a single addition (Fig. 6) and confirms that *C2M*

effectively maintains its performance gains in more complex kernels such as GEMV and GEMM.

We vary the number of banks from one to a maximum of 16. With a single bank, each step’s latency is considerably high, dictated by the tAAP + tRRD timing, allowing one AAP operation every AAP + tRRD. With 4 banks, we can overlap four AAP commands across different banks, each separated by tRRD. However, the delay between the first and fifth activation commands is still limited by tAAP + tRRD since the fifth can only start after the first finishes. For 16 banks, although constrained by the four activation window (FAW), the latency between the first and fifth activation is now bounded by tFAW, which is shorter than tAAP (tRAS + tRP + 4).

As shown in Fig. 11c, the single-bank configuration achieves the highest performance per Watt because it significantly reduces power, and increasing banks does not linearly scale throughput. However, the highest throughput is achieved with the 16-bank configuration.

Key results: On a number of different shapes GEMM and GEMV, *C2M* outperforms *SIMDRAM* by $2\times$ and $1.15\times$ in terms of latency and throughput and throughput per watt.

D. Comparison to GPU and the impact of predication

Fig. 12 presents throughput and throughput per Watt and area of *SIMDRAM*, *C2M*, and *PC2M*, all normalized to the GPU baseline. As expected, with GPUs and BLAS routines being particularly designed and hand-optimized for GEMM, the CIM accelerators exhibit lower throughput compared to the GPU. However, in terms of throughput per area and throughput per Watt, the *C2M* configurations still provide competitive results while the *PC2M:16* consistently outperforms GPU (and all other configurations, including *C2M*).

Note that all results for in-DRAM designs use a single rank with one subarray per bank doing the computations. The results scale linearly with increasing the number of CIM subarrays and ranks. Further, we are using conservative estimates with a typical tFAW of 30 ns. All-bank activation as suggested in prior work in the CIM domain [43], though this approach will clearly lead to superior throughput compared to GPU in all configurations, it incurs higher power consumption.

On the GEMV kernels, in-DRAM counting clearly outperforms GPU, with *PC2M* posting up to $100\times$ gains in terms

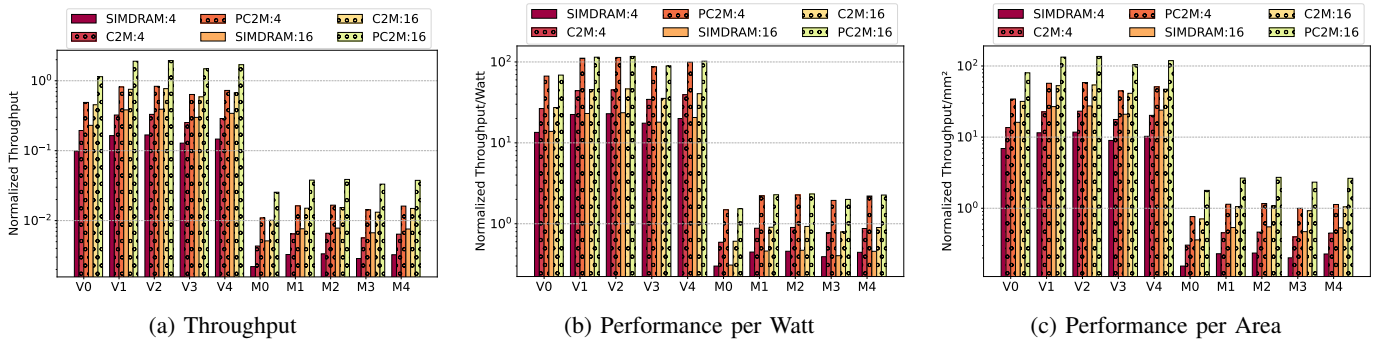


Fig. 12: GPU-normalized performance for real ternary GEMM and GEMV [37], [54], [55].

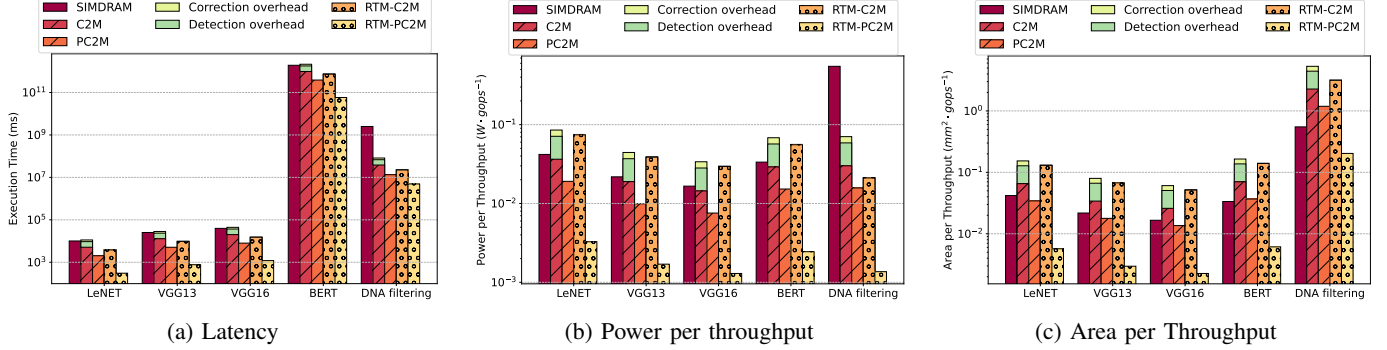


Fig. 13: Performance comparison of real-world workloads and protection scheme overhead.

of energy efficiency and performance density while delivering comparable throughput. Despite the added transistors increasing area and power compared *C2M*, *PC2M* demonstrates substantial gains in counting operations. Performance and energy savings achieved by the predicated RTM-based Count2Multiply will be discussed in the next section.

Key results: Compared to GPU, SIMD:4 in its best case is still an order of magnitude slower while *C2M* is either comparable (in throughput, with predication) or up to two orders of magnitude better (in GOPS/area and GOPS/watt).

E. Impact of the protection scheme on performance/energy

Fig. 13 compares *C2M* with and without protection, to the baseline SIMD:4 using five workloads, including TWNs, transformer model and DNA pre-alignment filtering. The impact of the protection scheme is twofold: 1) additional operations are needed to perform *detection* ($7n + 7 \rightarrow 13n + 16$), and 2) recomputation is required (*correction*) if a fault is detected. Detection rate, which informs efficiency overheads are reported in Table II. For more intuitive visualization of the protection overheads, we present the inverse in Fig. 13b-13c.

Estimating protection overhead requires the memory’s fault rate and the number of repetitions to be performed. In Fig. 13, we consider an inherent fault rate of 10^{-4} and 1 round of FC computation (repeats = 1). This translates to a detected fault rate of 3.5×10^{-4} per bit (Table II) and 0.16 per 512-bit row. As shown in Fig. 13, the correction overhead in DRAM designs is 19.6%, while it is insignificant in RTMs (0.001%).

RTMs offer competitive read/write speeds and the potential for higher performance compared to DRAM. However, as seen

in *RTM-C2M* bars, the high operation cost per increment leads to DRAM-based *PC2M* outperforming the non-predicate RTM implementation. Nonetheless, *RTM-PC2M* excels in all aspects, due to its constant increment function $f(n) = 3$, despite supporting only unit increments because of the transverse-write nature. Across all five workloads, *C2M* and *RTM-C2M* achieve a geomean speedup of $3\times$ and $7.6\times$, respectively, while delivering $1.4\times$ and $1.7\times$ higher throughput per Watt, and $1.4\times$ and $1.5\times$ higher throughput per area compared to protected SIMD:4. On some benchmarks, e.g., DNA filtering, our *PC2M* configurations are outperforming SIMD:4 by two to three orders of magnitude.

Despite the protection overhead, *PC2M* and *RTM-PC2M* configurations still achieve better results compared to SIMD:4. The (latency, performance per Watt, and performance per area) improvements translate to ($10\times$, $57\times$, and $3.8\times$) and ($25\times$, approx. $1\times$ and $5.6\times$), respectively. Note that the protection schemes do not apply to predicated versions.

Key results: *C2M*, despite the protection overhead, delivers considerable gains compared to the unprotected SIMD:4.

F. Counters radix selection

Varying counter radices significantly impacts, the counters’ overhead ($d \cdot n + 4$ rows per subarrays where n is radix/2), performance as demonstrated in Fig. 6, as well as the potential for CIM faults, presented as root mean squared error (RMSE) in Fig. 14. With JC encoding, additional faults can be detected simply by examining the state of the counters. For instance, in any valid JC state, there can only be one rising edge and one falling edge in the bit values from the MSB to the LSB.

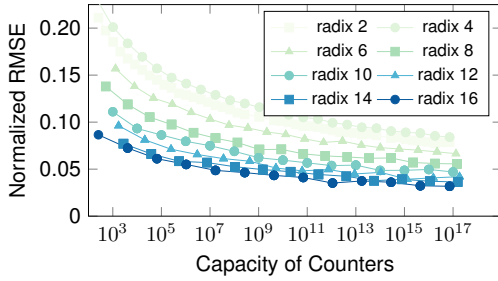


Fig. 14: Error exploration for random CIM faults on counters for different radices and count capacities.

Any other changes in the bit values will be an invalid JC state and indicate a fault. Any single-bit faults that can be detected can be corrected, but flips in the bits adjacent to the correct transition location cannot be detected. This indicates that faults in JCs with $R \in \{2, 4\}$ are never detectable. The impact of this principle on RMSE shows a significant reduction in error starting at $R = 6$ with diminishing returns after $R > 16$.

Key results: Radices in the range of 8–12 offer a good compromise for performance, overhead, and fault detection.

VII. CONCLUSIONS

We present Count2Multiply, a technology-independent digital-CIM method that facilitates integer-binary and integer-integer matrix multiplications using high-radix, massively parallel counting with bitwise logic operations. Count2Multiply considers reliability a first-class metric and presents a fault tolerance method that is compatible with existing ECC codes, minimizing detection and correction overheads. Unlike existing designs, Count2Multiply is technology-agnostic, as demonstrated by its implementations in DRAM and RTM. Compared to state-of-the-art in-DRAM methods, C2M and predicated PC2M deliver $3\times$ and $10\times$ speedups, respectively, with $1.4\times$ and $3.8\times$ higher throughput per Watt and $1.4\times$ and $1.02\times$ higher throughput per area. The predicated RTM counters delivers improvements of $10\times$ in latency, $57\times$ in GOPS/W, and $3.8\times$ in GOPS/mm².

ACKNOWLEDGMENTS

This work was partially funded by the Center for Advancing Electronics Dresden (cfaed) and the German Research Council (DFG) through the HetCIM project (502388442), CO4RTM project(450944241), and the AI competence center ScaDS.AI Dresden/Leipzig in Germany (01IS18026A-D).

REFERENCES

- [1] F. Aguirre, A. Sebastian, M. Le Gallo, W. Song, T. Wang, J. J. Yang, W. Lu, M.-F. Chang, D. Ielmini, Y. Yang *et al.*, “Hardware implementation of memristor-based artificial neural networks,” *Nature Communications*, vol. 15, no. 1, p. 1974, 2024.
- [2] M. F. Ali, A. Jaiswal, and K. Roy, “In-memory low-cost bit-serial addition using commodity dram technology,” *IEEE Transactions on Circuits and Systems I: Regular Papers*, vol. 67, no. 1, pp. 155–165, 2019.
- [3] L. Amarú, P.-E. Gaillardon, and G. De Micheli, “Majority-inverter graph: A novel data-structure and algorithms for efficient logic optimization,” in *Proceedings of the 51st Annual Design Automation Conference*, 2014, pp. 1–6.
- [4] S. Asif and M. Vesterbacka, “Performance analysis of radix-4 adders,” *Integration*, vol. 45, no. 2, pp. 111–120, 2012.
- [5] J. Batson, D. A. Spielman, N. Srivastava, and S.-H. Teng, “Spectral sparsification of graphs: theory and algorithms,” *Communications of the ACM*, vol. 56, no. 8, pp. 87–94, 2013.
- [6] R. Bläsing, A. A. Khan, P. C. Filippou, C. Garg, F. Hameed, J. Castrillon, and S. S. P. Parkin, “Magnetic racetrack memory: From physics to the cusp of applications within a decade,” *Proceedings of the IEEE*, vol. 108, no. 8, pp. 1303–1321, 2020.
- [7] A. Boroumand, S. Ghose, Y. Kim, R. Ausavarungnirun, E. Shiu, R. Thakur, D. Kim, A. Kuusela, A. Knies, P. Ranganathan *et al.*, “Google workloads for consumer devices: Mitigating data movement bottlenecks,” in *Proceedings of the Twenty-Third International Conference on Architectural Support for Programming Languages and Operating Systems*, 2018, pp. 316–331.
- [8] P. Brazzale, B. F. M. III, E. McKinney, P. Zhou, J. Hu, A. A. Khan, and A. K. Jones, “Towards error correction for computing in racetrack memory,” 2024. [Online]. Available: <https://arxiv.org/abs/2407.21661>
- [9] S. Cho and H. Lee, “Flip-n-write: A simple deterministic technique to improve pram write performance, energy and endurance,” in *Proceedings of the 42nd Annual IEEE/ACM International Symposium on Microarchitecture*, 2009, pp. 347–357.
- [10] H.-j. Chung, C.-S. Park, T.-Y. Oh, J.-W. Ryu, C.-Y. Lee, T.-S. Jang, and G.-H. Han, “Memory devices that perform masked write operations and methods of operating the same,” Mar. 7 2017, uS Patent 9,588,840.
- [11] H. Cilasun, S. Resch, Z. I. Chowdhury, M. Zabihi, Y. Lv, B. Zink, J.-P. Wang, S. S. Sapatnekar, and U. R. Karpuzcu, “On error correction for nonvolatile processing-in-memory,”
- [12] N. Corporation, “Nvidia geforce rtx 3090 whitepaper,” <https://www.nvidia.com/content/PDF/nvidia-ampere-ga-102-gpu-architecture-whitepaper-v2.pdf>, 2020, accessed: 2024-08-01.
- [13] Q. Deng, L. Jiang, Y. Zhang, M. Zhang, and J. Yang, “Dracc: A dram based accelerator for accurate cnn inference,” in *Proceedings of the 55th annual design automation conference*, 2018, pp. 1–6.
- [14] P. Dutta, A. Lee, K. L. Wang, A. K. Jones, and S. Bhanja, “A multi-domain magneto tunnel junction for racetrack nanowire strips,” *IEEE Transactions on Nanotechnology*, vol. 22, pp. 581–583, 2023.
- [15] C. Eckert, X. Wang, J. Wang, A. Subramanian, R. Iyer, D. Sylvester, D. Blaauw, and R. Das, “Neural cache: Bit-serial in-cache acceleration of deep neural networks,” in *2018 ACM/IEEE 45th annual international symposium on computer architecture (ISCA)*. IEEE, 2018, pp. 383–396.
- [16] F. Gao, G. Tziantzioulis, and D. Wentzlaff, “Computedram: In-memory compute using off-the-shelf drams,” in *Proceedings of the 52nd Annual IEEE/ACM International Symposium on Microarchitecture*, ser. MICRO ’52. New York, NY, USA: Association for Computing Machinery, 2019, p. 100–113. [Online]. Available: <https://doi.org/10.1145/3352460.3358260>
- [17] A. Gholami, S. Kim, Z. Dong, Z. Yao, M. W. Mahoney, and K. Keutzer, “A survey of quantization methods for efficient neural network inference,” in *Low-Power Computer Vision*. Chapman and Hall/CRC, 2022, pp. 291–326.
- [18] N. Hajinazar, G. F. Oliveira, S. Gregorio, J. a. D. Ferreira, N. M. Ghiasi, M. Patel, M. Alser, S. Ghose, J. Gómez-Luna, and O. Mutlu, “Simdram: a framework for bit-serial simd processing using dram,” in *Proceedings of the 26th ACM International Conference on Architectural Support for Programming Languages and Operating Systems*, ser. ASPLOS ’21. New York, NY, USA: Association for Computing Machinery, 2021, p. 329–345. [Online]. Available: <https://doi.org/10.1145/3445814.3446749>
- [19] F. Hameed, A. A. Khan, and J. Castrillon, “Performance and energy-efficient design of stt-ram last-level cache,” *IEEE Transactions on Very Large Scale Integration (VLSI) Systems*, vol. 26, no. 6, pp. 1059–1072, June 2018.
- [20] F. Hameed, A. Khan, and J. Castrillon, “ALPHA: A Novel Algorithm-Hardware Co-design for Accelerating DNA Seed Location Filtering,” *IEEE Transactions on Emerging Topics in Computing*, pp. 1–1, 2021.
- [21] Y.-S. Hsiao, S. K. S. Hari, B. Sundaralingam, J. Yik, T. Tambe, C. Sakr, S. W. Keckler, and V. J. Reddi, “Vapr: Variable-precision tensors to accelerate robot motion planning,” in *2023 IEEE/RSJ International Conference on Intelligent Robots and Systems (IROS)*. IEEE, 2023, pp. 6304–6309.
- [22] I. Hubara, M. Courbariaux, D. Soudry, R. El-Yaniv, and Y. Bengio, “Binarized neural networks,” *Advances in neural information processing systems*, vol. 29, 2016.
- [23] A. Keprt, “Binary matrix pseudo-division and its applications,” in *Innovations in Bio-inspired Computing and Applications: Proceedings of the 4th International Conference on Innovations in Bio-Inspired*

Computing and Applications, IBICA 2013, August 22-24, 2013-Ostrava, Czech Republic. Springer, 2014, pp. 153–164.

- [24] A. A. Khan, F. Hameed, R. Bläsing, S. Parkin, and J. Castrillon, “RTSim: A Cycle-Accurate Simulator for Racetrack Memories,” *IEEE Computer Architecture Letters*, vol. 18, no. 1, pp. 43–46, Jan 2019.
- [25] A. A. Khan, S. Ollivier, S. Longofono, G. Hempel, J. Castrillon, and A. K. Jones, “Brain-inspired cognition in next generation racetrack memories,” *ACM Trans. Embed. Comput. Syst.*, mar 2022. [Online]. Available: <https://doi.org/10.1145/3524071>
- [26] A. I. Khan, A. Keshavarzi, and S. Datta, “The future of ferroelectric field-effect transistor technology,” *Nature Electronics*, vol. 3, no. 10, pp. 588–597, 2020.
- [27] J. Kim, D. Senol Cali, H. Xin, D. Lee, S. Ghose, M. Alser, H. Hassan, O. Ergin, C. Alkan, and O. Mutlu, “GRIM-Filter: Fast Seed Location Filtering in DNA Read Mapping using Processing-in-memory Technologies,” *BMC Genomics*, vol. 19, no. 2, 2018.
- [28] S. Kvatinsky, D. Belousov, S. Liman, G. Satat, N. Wald, E. G. Friedman, A. Kolodny, and U. C. Weiser, “Magic—memristor-aided logic,” *IEEE Transactions on Circuits and Systems II: Express Briefs*, vol. 61, no. 11, pp. 895–899, 2014.
- [29] M. Le Gallo, R. Khaddam-Aljameh, M. Stanisavljevic, A. Vasilopoulos, B. Kersting, M. Dazzi, G. Karunaratne, M. Brändli, A. Singh, S. M. Mueller *et al.*, “A 64-core mixed-signal in-memory compute chip based on phase-change memory for deep neural network inference,” *Nature Electronics*, vol. 6, no. 9, pp. 680–693, 2023.
- [30] L. Lee, “Fast context-free grammar parsing requires fast boolean matrix multiplication,” *Journal of the ACM (JACM)*, vol. 49, no. 1, pp. 1–15, 2002.
- [31] F. Li, B. Liu, X. Wang, B. Zhang, and J. Yan, “Ternary weight networks,” *arXiv preprint arXiv:1605.04711*, 2016.
- [32] S. Li, D. Niu, K. T. Malladi, H. Zheng, B. Brennan, and Y. Xie, “Drisa: A dram-based reconfigurable in-situ accelerator,” in *2017 50th Annual IEEE/ACM International Symposium on Microarchitecture (MICRO)*. IEEE, 2017, pp. 288–301.
- [33] S. Li, C. Xu, Q. Zou, J. Zhao, Y. Lu, and Y. Xie, “Pinatubo: A processing-in-memory architecture for bulk bitwise operations in emerging non-volatile memories,” in *2016 53rd ACM/EDAC/IEEE Design Automation Conference (DAC)*, 2016, pp. 1–6.
- [34] Y. Li, X. Dong, S. Q. Zhang, H. Bai, Y. Chen, and W. Wang, “Rtn: Reparameterized ternary network,” in *Proceedings of the AAAI Conference on Artificial Intelligence*, vol. 34, no. 04, 2020, pp. 4780–4787.
- [35] B. Liu, S. Gu, M. Chen, W. Kang, J. Hu, Q. Zhuge, and E. H.-M. Sha, “An efficient racetrack memory-based processing-in-memory architecture for convolutional neural networks,” in *2017 IEEE International Symposium on Parallel and Distributed Processing with Applications and 2017 IEEE International Conference on Ubiquitous Computing and Communications (ISPA/IUCC)*. IEEE, pp. 383–390.
- [36] S.-L. Lu, Y.-C. Lin, and C.-L. Yang, “Improving dram latency with dynamic asymmetric subarray,” in *Proceedings of the 48th International Symposium on Microarchitecture*, 2015, pp. 255–266.
- [37] S. Ma, H. Wang, L. Ma, L. Wang, W. Wang, S. Huang, L. Dong, R. Wang, J. Xue, and F. Wei, “The era of 1-bit llms: All large language models are in 1.58 bits,” *arXiv preprint arXiv:2402.17764*, 2024.
- [38] G. F. Oliveira, A. Olgun, A. G. Yağlıkçı, F. N. Bostancı, J. Gómez-Luna, S. Ghose, and O. Mutlu, “Mimdram: An end-to-end processing-using-dram system for high-throughput, energy-efficient and programmer-transparent multiple-instruction multiple-data computing,” in *2024 IEEE International Symposium on High-Performance Computer Architecture (HPCA)*. IEEE, 2024, pp. 186–203.
- [39] S. Ollivier, S. Longofono, P. Dutta, J. Hu, S. Bhanja, and A. K. Jones, “CORUSCANT: Fast efficient processing-in-racetrack memories,” in *55th IEEE/ACM International Symposium on Microarchitecture (MICRO)*, October 2022, [preprint appears online] <https://arxiv.org/abs/2108.01202>.
- [40] S. Ollivier, S. Longofono, P. Dutta, J. Hu, S. Bhanja, and A. K. Jones, “Toward comprehensive shifting fault tolerance for domain-wall memories with pielt,” *IEEE Transactions on Computers*, pp. 1–14, 2022.
- [41] S. Ollivier, X. Zhang, Y. Tang, C. Choudhuri, J. Hu, and A. K. Jones, “POD-RACING: Bulk-bitwise to floating-point compute in racetrack memory for machine learning at the edge,” *IEEE Micro*, 2022, [preprint appears online] <https://arxiv.org/abs/2204.13788>. [Online]. Available: <https://arxiv.org/abs/2204.13788>
- [42] P. A. K. H. C. R., and P. P., “Method to handle write mask in dram memory,” Mar. 7 2010, china Patent CN101176159A.
- [43] Y. Paik, C. H. Kim, W. J. Lee, and S. W. Kim, “Achieving the performance of all-bank in-dram pim with standard memory interface: Memory-computation decoupling,” *IEEE Access*, vol. 10, pp. 93 256–93 272, 2022.
- [44] X. Peng, Y. Wang, and M.-C. Yang, “Chopper: A compiler infrastructure for programmable bit-serial simd processing using memory in dram,” in *2023 IEEE International Symposium on High-Performance Computer Architecture (HPCA)*. IEEE, 2023, pp. 1275–1288.
- [45] M. Poremba, T. Zhang, and Y. Xie, “Nvmain 2.0: A user-friendly memory simulator to model (non-)volatile memory systems,” *IEEE Computer Architecture Letters*, vol. 14, no. 2, pp. 140–143, July 2015.
- [46] H. Qin, R. Gong, X. Liu, X. Bai, J. Song, and N. Sebe, “Binary neural networks: A survey,” *Pattern Recognition*, vol. 105, p. 107281, 2020.
- [47] E. Reggiani, A. Pappalardo, M. Doblas, M. Moreto, M. Olivieri, O. S. Unsal, and A. Cristal, “Mix-gemm: An efficient hw-sw architecture for mixed-precision quantized deep neural networks inference on edge devices,” in *2023 IEEE International Symposium on High-Performance Computer Architecture (HPCA)*. IEEE, 2023, pp. 1085–1098.
- [48] K. Roxy, S. Ollivier, A. Hoque, S. Longofono, A. K. Jones, and S. Bhanja, “A novel transverse read technique for domain-wall “race-track” memories,” *IEEE Transactions on Nanotechnology*, vol. 19, pp. 648–652, 2020.
- [49] S. Roy, M. Ali, and A. Raghunathan, “Pim-dram: Accelerating machine learning workloads using processing in commodity dram,” *IEEE Journal on Emerging and Selected Topics in Circuits and Systems*, vol. 11, no. 4, pp. 701–710, 2021.
- [50] T. Schwarz and C. Hochberger, “Memristor based fpgas: Understanding the effect of configuration memory faults,” in *Architecture of Computing Systems*, M. Schulz, C. Trinitis, N. Papadopoulou, and T. Pionteck, Eds. Cham: Springer International Publishing, 2022, pp. 167–180.
- [51] V. Seshadri, Y. Kim, C. Fallin, D. Lee, R. Ausavarungnirun, G. Pekhimenko, Y. Luo, O. Mutlu, P. B. Gibbons, M. A. Kozuch *et al.*, “Rowclone: Fast and energy-efficient in-dram bulk data copy and initialization,” in *Proceedings of the 46th Annual IEEE/ACM International Symposium on Microarchitecture*, 2013, pp. 185–197.
- [52] V. Seshadri, D. Lee, T. Mullins, H. Hassan, A. Boroumand, J. Kim, M. A. Kozuch, O. Mutlu, P. B. Gibbons, and T. C. Mowry, “Ambit: In-memory accelerator for bulk bitwise operations using commodity dram technology,” in *2017 50th Annual IEEE/ACM International Symposium on Microarchitecture (MICRO)*, 2017, pp. 273–287.
- [53] K. Smagulova, M. E. Fouda, F. Kurdahi, K. N. Salama, and A. Eltawil, “Resistive neural hardware accelerators,” *Proceedings of the IEEE*, vol. 111, no. 5, pp. 500–527, 2023.
- [54] H. Touvron, T. Lavril, G. Izacard, X. Martinet, M.-A. Lachaux, T. Lacroix, B. Rozière, N. Goyal, E. Hambro, F. Azhar *et al.*, “Llama: Open and efficient foundation language models,” *arXiv preprint arXiv:2302.13971*, 2023.
- [55] H. Touvron, L. Martin, K. Stone, P. Albert, A. Almahairi, Y. Babaei, N. Bashlykov, S. Batra, P. Bhargava, S. Bhosale *et al.*, “Llama 2: Open foundation and fine-tuned chat models,” *arXiv preprint arXiv:2307.09288*, 2023.
- [56] M. S. Q. Truong, E. Chen, D. Su, L. Shen, A. Glass, L. R. Carley, J. A. Bain, and S. Ghose, “Racer: Bit-pipelined processing using resistive memory,” in *MICRO-54: 54th Annual IEEE/ACM International Symposium on Microarchitecture*, ser. MICRO ’21. New York, NY, USA: Association for Computing Machinery, 2021, p. 100–116. [Online]. Available: <https://doi.org/10.1145/3466752.3480071>
- [57] I. Vourkas, G. C. Sirakoulis, I. Vourkas, and G. C. Sirakoulis, “High-radix arithmetic-logic unit (alu) based on memristors,” *Memristor-Based Nanoelectronic Computing Circuits and Architectures*, pp. 149–172, 2016.
- [58] L. Wang, L. Ma, S. Cao, Q. Zhang, J. Xue, Y. Shi, N. Zheng, Z. Miao, F. Yang, T. Cao, Y. Yang, and M. Yang, “Ladder: Enabling efficient low-precision deep learning computing through hardware-aware tensor transformation,” in *18th USENIX Symposium on Operating Systems Design and Implementation (OSDI 24)*, 2024. [Online]. Available: <https://www.usenix.org/conference/osdi24/presentation/wang-lei>
- [59] H. . P. Wong, H. Lee, S. Yu, Y. Chen, Y. Wu, P. Chen, B. Lee, F. T. Chen, and M. Tsai, “Metal-oxide rram,” *Proceedings of the IEEE*, vol. 100, no. 6, pp. 1951–1970, June 2012.

- [60] H.-S. P. Wong, S. Raoux, S. Kim, J. Liang, J. Reifenberg, B. Rajendran, M. Asheghi, and K. Goodson, "Phase change memory," *Proceedings of the IEEE*, vol. 98, 12 2010.
- [61] X. Xin, Y. Zhang, and J. Yang, "Elp2im: Efficient and low power bitwise operation processing in dram," in *2020 IEEE International Symposium on High Performance Computer Architecture (HPCA)*. IEEE, 2020, pp. 303–314.
- [62] B.-D. Yang, J.-E. Lee, J.-S. Kim, J. Cho, S.-Y. Lee, and B.-G. Yu, "A low power phase-change random access memory using a data-comparison write scheme," in *2007 IEEE International Symposium on Circuits and Systems (ISCAS)*, 2007, pp. 3014–3017.
- [63] H. You, X. Chen, Y. Zhang, C. Li, S. Li, Z. Liu, Z. Wang, and Y. Lin, "Shiftaddnet: A hardware-inspired deep network," *Advances in Neural Information Processing Systems*, vol. 33, pp. 2771–2783, 2020.
- [64] I. E. Yuksel, Y. C. Tugrul, A. Olgun, F. N. Bostanci, A. G. Yağlıkçı, G. F. Oliveira, H. Luo, J. Gómez-Luna, M. Sadrosadati, and O. Mutlu, "Functionally-complete boolean logic in real dram chips: Experimental characterization and analysis," in *2024 IEEE International Symposium on High-Performance Computer Architecture (HPCA)*, 2024, pp. 280–296.
- [65] R. Zhou, A. Roohi, D. Misra, and S. Angizi, "Flexidram: A flexible in-dram framework to enable parallel general-purpose computation," in *Proceedings of the ACM/IEEE International Symposium on Low Power Electronics and Design*, 2022, pp. 1–6.